A Seasonal and Spatial Study of Upwelling Dynamics and Coastal Atmospheric pCO_2 in Monterey Bay, CA

Diego Sancho, Stanford University

Mentors: Francisco P. Chavez

Summer 2017

Keywords: Upwelling, coastal atmospheric pCO_2, Monterey Bay, seasonality, spatial gradient, time series

ABSTRACT

Time series data from three moorings in waters near Monterey Bay, CA during the 2014-2017 period were used to examine seasonal and spatial variation of temperature, salinity, pCO_2 in seawater, pH and dissolved oxygen in response to upwelling-inducing northwesterly winds. Data were also used to investigate the seasonal and spatial effects of anthropogenic atmospheric pCO_2 in the coastal ocean in this region. Analyses of lagged cross-covariance, band-pass filters, and data interpolation were used to quantify the responses of ocean parameters to upwelling winds. CO_2 flux calculations were used to determine the impact of heavily CO_2 polluted coastal air on seawater. Analyses determine that upwelling is a highly seasonal phenomenon, occurring in the spring and early summer strongly affecting the regions closest to the upwelling center near Año Nuevo State Park, CA. Duration, intensity and impact of upwelling events in seawater is proportional to the duration of the northwesterly winds that drive upwelling and the distance from the upwelling center. Upwelling events have a duration of 3-7 days with highest temperature, pCO_{2w}, O_2 and pH amplitude and variability at Año Nuevo (OA2), intermediate amplitude and variability at M1, and lowest amplitude and variability at Hopkins (OA1). A transient signal of heavily carbon dioxide polluted coastal air, on top of the global anthropogenic trend, is present in the three moorings, especially during the

winter season. The impact of the heavily polluted coastal air is to increase the absorption of CO_2 by the ocean at all locations with decreasing impact as distance from shore increases. This coastal ocean absorption is neglected in present coastal air-sea flux estimates. Longer time series observations in the future will allow for more complex and nuanced analyses of the ocean's large-scale processes.

INTRODUCTION

The Central California Current System is one of the most biologically productive regions in the world (Kudela et al., 2008). The oceanography of this region is strongly influenced by the process of coastal upwelling (Service et al., 1998; Pennington & Chavez, 2000; Kudela et al., 2008). Southward wind stress along the US West Coast drives an offshore Ekman layer flux that is balanced by the upwelling of cold, nutrient-rich water from depth (Kudela et al., 2008). Upwelling in Monterey Bay, CA occurs primarily in the spring and early summer, when a band of cold, low-pH, deoxygenated water develops from upwelling centers near the coast (Skosberg, 1936; Skosberg & Phelps, 1946; Rosenfeld et al., 1994; Pennington & Chavez, 2000). This process is critical to sustain the complex biological system that thrives in Monterey Bay (Barber and Smith, 1981; Chavez et al., 1991).

Studies of upwelling have focused on a time series approach that describes changes over time in the oceanography of Monterey Bay (Service et al., 1998; Pennington & Chavez, 2000; Pennington & Chavez, 2017). Due to the complex current flow inside Monterey Bay (Rosenfeld et al., 1994; Graham & Largier, 1995; Drake et al., 2005), the effects of upwelling are wide-ranging and localized for each temporal and spatial evolution of the upwelling process within Monterey Bay. Similar to upwelling, coastal atmospheric carbon dioxide is measured by the same array of sensors installed on oceanographic moorings. Thus, measurements of atmospheric CO_2 over time and space are also available. These critical observations can inform on the effect of atmospheric CO_2 in the upwelling coastal ocean by quantifying air-sea fluxes in this environment (Bakker et al., 1996; Carvalho et al., 2011). This investigation of atmospheric carbon dioxide and upwelling dynamics aims to describe and compare over space and time these key indicators of present and future change in the coastal ocean.

Time series data for this project were obtained from a number of buoys near Monterey Bay, CA operated by the Monterey Bay Aquarium Research Institute (MBARI) that provide routine measurements of physical, chemical, and biological properties of the upper ocean and atmosphere. Each buoy is equipped with sensors to measure ocean and atmosphere properties such as temperature, salinity, pH, pCO_2 in air and water, O_2 in water, fluorescence, and wind speed and direction. This project focuses on the description and analyses of the data sets available for the OA1, OA2 and M1 buoys.

OA1 (Hopkins) is located ~100 m offshore of Hopkins Marine Station in Point Cabrillo, Monterey, CA, and has been in operation since March 2012 (Fig.1). **OA2 (Año Nuevo)** is located ~300 m offshore of Año Nuevo Island in Año Nuevo State Park, CA (Fig. 1). This mooring was initially deployed in April 2011 near Terrace Point in Santa Cruz, CA, and was moved to its current location off Año Nuevo in May 2015. Temperature, salinity, depth, O_2, fluorescence and pH measurements at OA1 and OA2 are taken every 15 min; pCO_2 and MET measurements are taken every hour. **M1** is located 18 km offshore of Moss Landing, CA above the Monterey Canyon in ~1000 m of water (Fig. 1). Regular measurements at M1 began in 1997, providing perhaps the most comprehensive time-series of carbon dioxide in a coastal system (Friederich et al., 2002). Temperature, salinity, depth, O_2, fluorescence and pH at M1 are measured every 15 minutes; pCO_2 is measured every hour, and MET every 10 minutes.

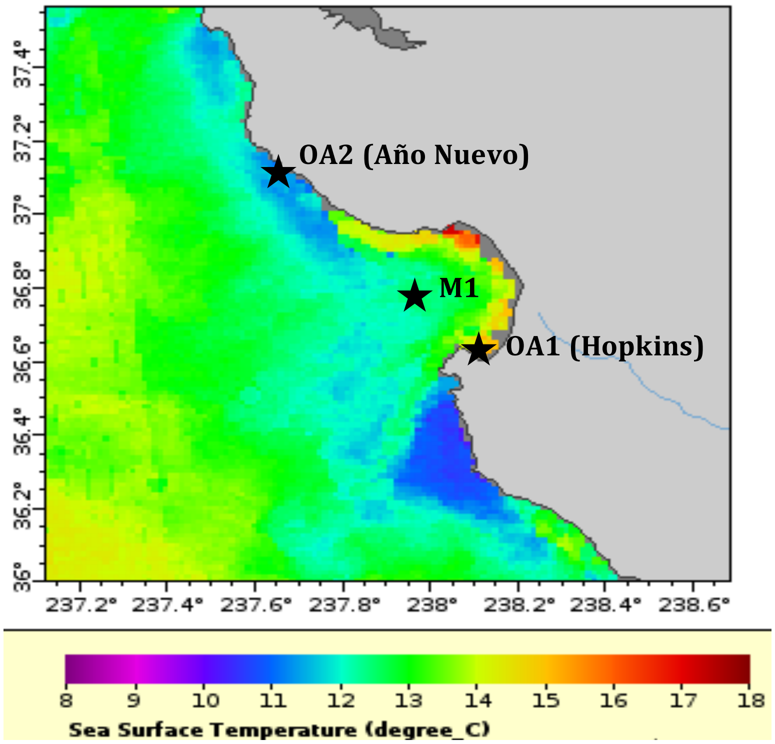

Figure 1. Map of sea surface temperature (°C) including mooring locations.

METHODS

1. Principal Component Analysis

Principal component winds were calculated from wind direction and speed measurements from each buoy. This analysis, also known as Empirical Orthogonal Function (EOF) Analysis, partitions the variance in wind speed and direction into a set of orthogonal axes. Subsequent statistical analyses of wind data are performed relative to the positive or negative wind speed along the principal axis of each mooring established by the principal component analyses.

2. Lagged Cross-covariance

In order to quantitatively relate the responses in physical, chemical, and biological variables to physical forcing by winds, a MATLAB script calculating lagged cross-covariance was created. Cross-covariance was used to measure the similarity between the principal axis of winds and the corresponding time-shifted (lagged) indices of temperature, salinity, pH, pCO_2 in air and seawater, O_2 in water, and fluorescence as a function of the lag, after the removal of sample means. Lags were calculated for correlations occurring within a week (±168 hours) based on the approximate average span of upwelling events in Monterey Bay (Service et al., 1998).

3. Band-pass Filters

Band-pass filters were implemented to determine the amplitudes of changes in the physical, biological and chemical variables occurring over discrete, pre-selected time focusing on diurnal and upwelling-induced variability. The frequency of the filters was determined by a wind spectra analysis including buoy NDBC 46042, found further offshore of Monterey Bay, for data validation. A 23-25 hour (daily) and a 3-7 day (upwelling event scale) filter were applied to all variables at each of the three moorings. OA1 and OA2 were filtered following the hourly time stamp of their MET data; M1 was filtered at a 10-minute measurement interval corresponding to its MET data time stamp. The nyquist frequency, or the minimum rate at which a signal can be sampled without inducing errors, was used to normalize the filter frequency. Maximum amplitude of each filtered time series was calculated to compare all of the variables for each buoy.

4. Data Manipulation

Wind direction was rotated along its principal axis to yield values that increase from NW-SE, and is referred to as "Northwesterly Wind Speed" in the figures below. For each buoy, all data were aligned temporally to the time stamp of the OA2 MET sensor using nearest-neighbor interpolation, to standardize CTD sampling to an hourly rate and fill short gaps in data collection caused by sensor malfunction. Two time periods were chosen for focused analyses based on local climatological data availability for the three moorings. Due to failure of the MET sensor at OA2 on December 7, 2015, wind data available at the three sites is limited to May 14, 2015 – December 7, 2015 and September 18, 2016 – June 29, 2017.

Large (month-long) gaps in pH at OA1 and M1 were filled by calculating pH from measurements of pCO_2 (when available) and estimates of total alkalinity (TA) derived from salinity (S) (TA = 2150 + 44*(S-31.25)) using the software package CO2SYS (van Heuven et al., 2011).

5. Coastal atmospheric pCO_2

Atmospheric pCO_2 measurements at each mooring were compared to global monthly mean levels of atmospheric pCO_2 as estimated by NOAA's Earth System

Research Laboratory. A 3-month gap with respect to the mooring measurements at the end of the global monthly mean dataset was filled by a second-degree polynomial extrapolation. Air-sea fluxes were calculated as $FCO_2 = k\ Sol\ \Delta pCO_2$, where k is the gas transfer rate (cm h^{-1}) computed following Wanninkhof (1992), *Sol* is the solubility in seawater (mol kg^{-1} atm^{-1}) computed following Weiss (1974), and $\Delta pCO_2 = pCO_{2w} - \Delta pCO_{2a}$ (μatm) where subscripts *w* and *a* refer to water and air, respectively. For the calculations of the *k* and *Sol* terms, wind and CTD data were linearly interpolated to the sample times of the CO_2 sensor, and wind speed measurements taken 1 m above sea level normalized to the standard reference height of 10 m following Large and Pond (1981).

CO_2 fluxes were estimated for the wintertime by calculating their monthly average, from November to February, for every year where data are available. Differences between sensor measurements and background levels of atmospheric pCO_2, also referred to as residual pCO_{2a}, were calculated by averaging pCO_{2a} at each mooring by month and subtracting the global atmospheric mean. CO_2 fluxes assuming an unpolluted atmosphere were calculated using background levels of atmospheric pCO_2, as opposed to mooring sensor measurements.

RESULTS and DISCUSSION

The time series for the entire data set (Fig. 1) shows where there are data available for the three moorings during February 2014 – July 2017. Although not temporally continuous, the two time periods used for analyses encompass every season present in Monterey Bay (Fig. 2. Skosberg, 1936; Skosberg & Phelps, 1946; Pennington & Chavez, 2000).

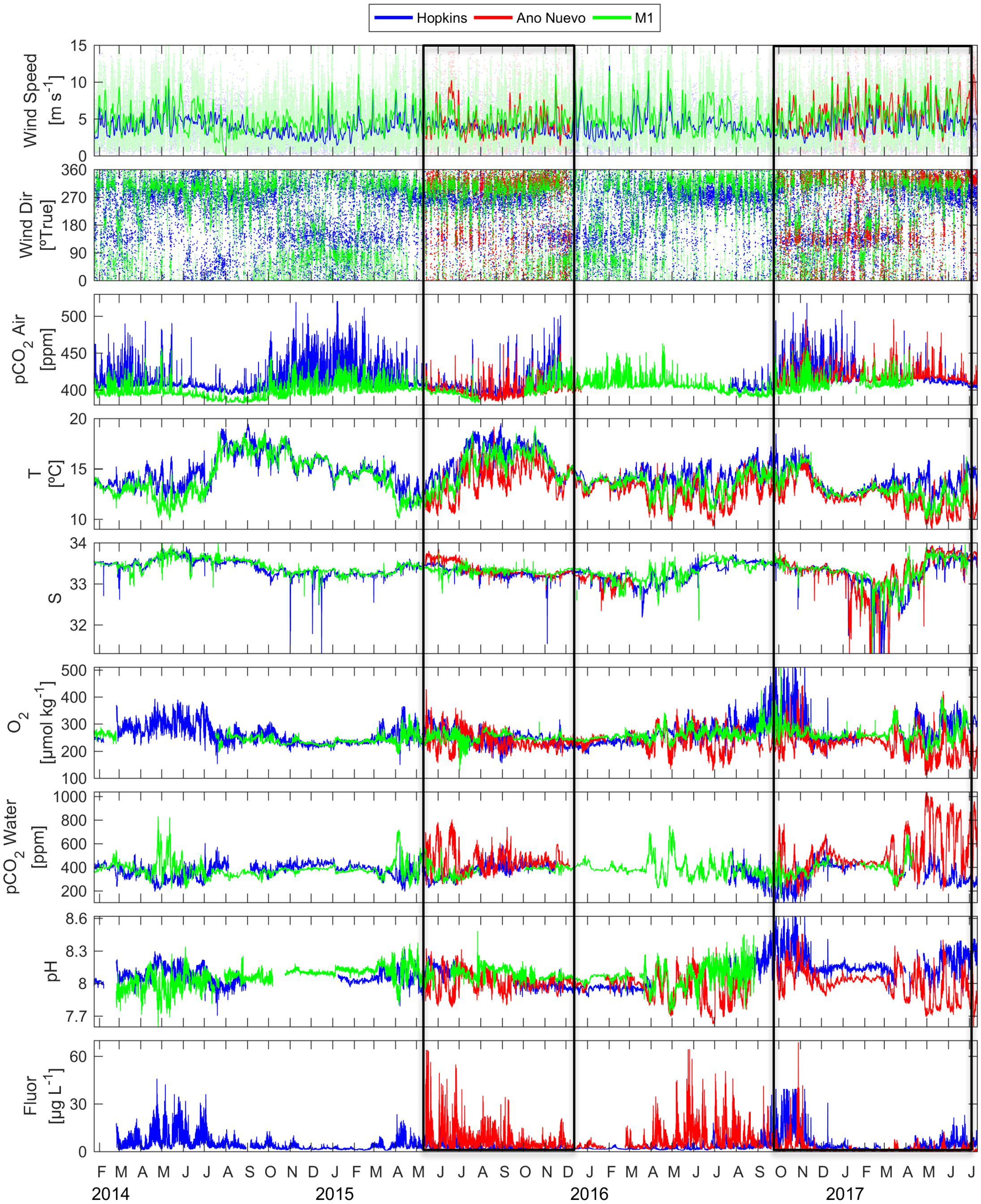

Figure 2. Time series of sensor measurements at the three buoys for the complete dataset (February 2014–July 2017). The darker lines highlight the periods chosen for in-depth analyses.

1. Time series observations from May 2015 – December 2015

The principal axes of winds at OA1, OA2, and M1, were oriented at 287°, 315°, and 295° True respectively, reflecting the general NW-SE pattern typical to this region (Strub et al., 1987) and also highlighting local variability due to proximity and shape of the coastline (Chao et al., 2003). The principal axis of winds for each mooring was used for the subsequent observations in this study.

At each mooring sensors measure different effects of upwelling, evidenced by the amplitude in the measurements recorded at each location. OA1 has relatively lower parameter variability than OA2 and M1 (Fig. 3), most likely due to the buoy's location in the shadow of the Monterey peninsula. Large changes in ocean temperature at OA1 are mainly associated with wind variability; in particular, warmer water during wind-relaxation periods that results in long-residence bay waters moving towards Hopkins from the nearshore environment in the lee of the peninsula (Paduan & Rosenfeld, 1996).

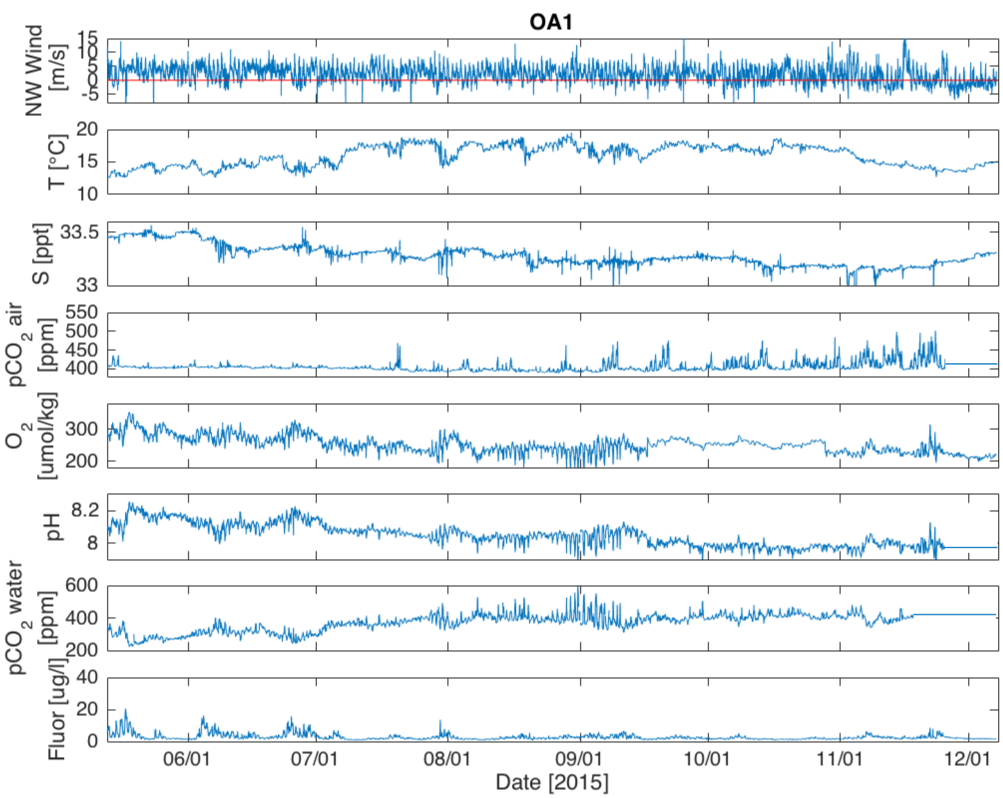

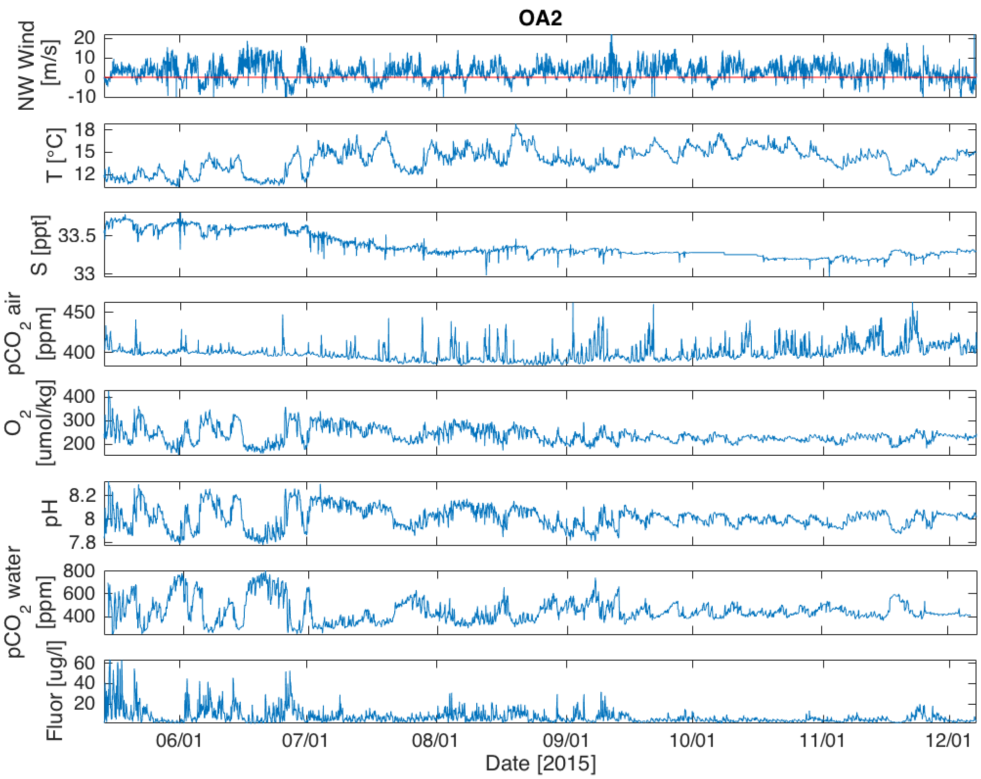

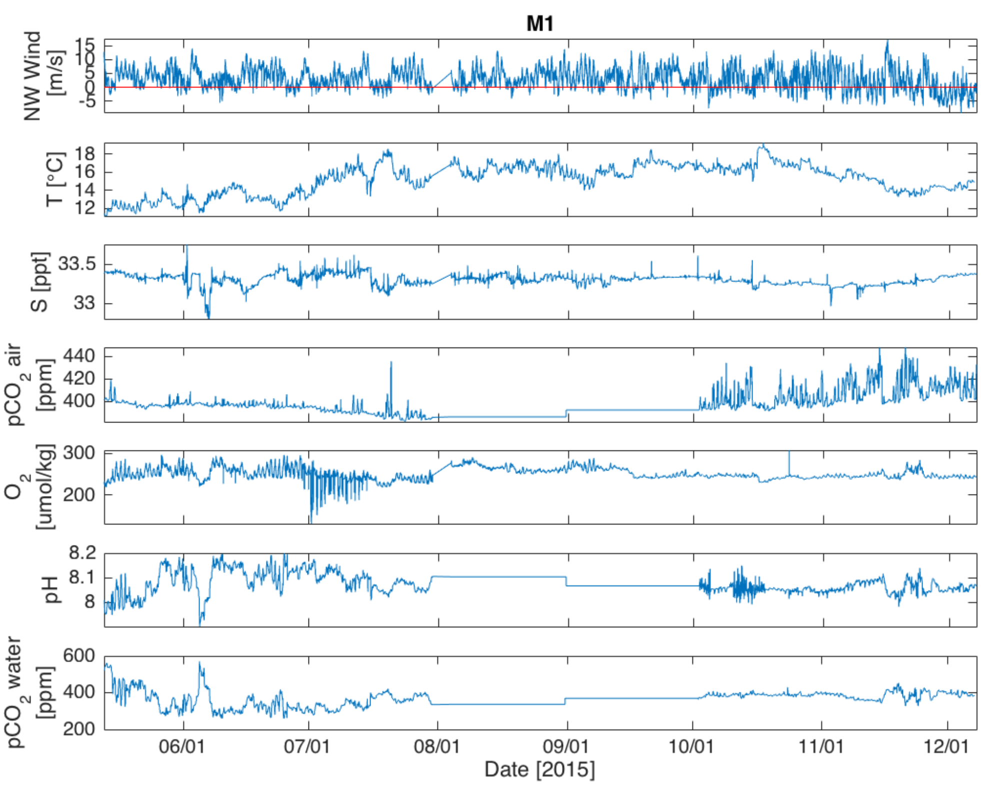

Figure 3. Time series of the three buoys for the May 13 – December 7, 2015 time period.

The amplitudes of the OA2 (Año Nuevo) variables are larger than those of OA1 (Hopkins) in most cases, particularly during the upwelling season. Temperature variability follows a 3-7 day pattern that reflects the time scale observed during upwelling events. These events can lead to changes in temperature ranging from 1-4 °C, lasting between 2 and 8 days depending on the duration of strong northwesterly winds. These abrupt rates of change in observed measurements evidence the occurrence of advective processes at OA2, an indicator of proximity to an upwelling center (Rosenfeld et al., 1994; Pennington & Chavez, 2000).

M1 follows a similar pattern as OA2, characterized by its large wind variability along its principal axis and corresponding variance in some of the measured variables. The amplitudes of the temperature curve are very similar to those of OA2, which evidence the effects of upwelling on the M1 mooring as described by Pennington & Chavez (2000). The duration of these events is similar to those observed at OA2. However, pH, oxygen and pCO_{2w} appear more stable at M1 than at OA2 due to its relative distance downstream from the upwelling center near Año Nuevo (Rosenfeld et al., 1994), over which biological processes like phytoplankton growth and assisted CO_2 drawdown in the ocean occur (Pennington & Chavez, 2000).

There is also evidence of seasonal variability, with stronger negative (southeasterly) winds as winter approaches, a signal of the transition into the "oceanic season" (Skosberg, 1936; Skosberg & Phelps, 1946; Pennington & Chavez, 2000). The time series show the end of the spring/summer upwelling season and beginning of the summer/fall oceanic season, where increased temperatures are observed and salinity decreases, potentially into the winter "Davidson Current" season, where salinity remains low and temperatures are colder relative to the oceanic period but warmer than during the upwelling season (Skosberg, 1936; Skosberg & Phelps, 1946; Pennington & Chavez, 2000). Similar seasonal patterns are observed in pH, pCO_{2w}, fluorescence and oxygen. OA2 and M1 measurements show greater variability in the upwelling season that stabilizes as the time series moves to winter. OA1 has greater variability on a weekly time scale during the upwelling season, but its main mode of change appears to be on a 24-hour basis. Paduan & Rosenfeld (1996) and Pennington & Chavez (2000) describe the stabilizing that occurs during the Davidson Current season as a result of winds and currents shifting northward with the inshore movement of the California Current waters and weakening of equatorward winds.

Atmospheric pCO_2 is influenced strongly by the strengthening of southerly winds, as concentrations increase in the seasonal transition into the Davidson Current. There is a particularly strong signal at OA1 due to its proximity to a coastal urban area. The measured rates of change of air pCO_2 at OA1 can reach up to 100 ppm in a day. This same pattern, at smaller amplitudes, can be observed for OA2 and M1, with rates of change that do not exceed 50 ppm in a day.

2. Time series observations from October 2016 – July 2017

The principal axes of winds at OA1, OA2, and M1, for this time period were oriented at 308°, 336°, and 330° True respectively. These values are shifted northward with respect to the previous time period (May-Dec 2015), but still reflect the general NW-SE pattern typical to this region (Strub et al., 1987) and local variability due to proximity and shape of the coastline (Chao et al., 2003).

This time period (Fig. 4) complements the first analyses (Fig. 3, May-Dec) with data from the winter and spring. The patterns in variability and strength of the upwelling signal remain similar to those described previously, but the data allow for equally detailed analyses of the full winter and spring time series.

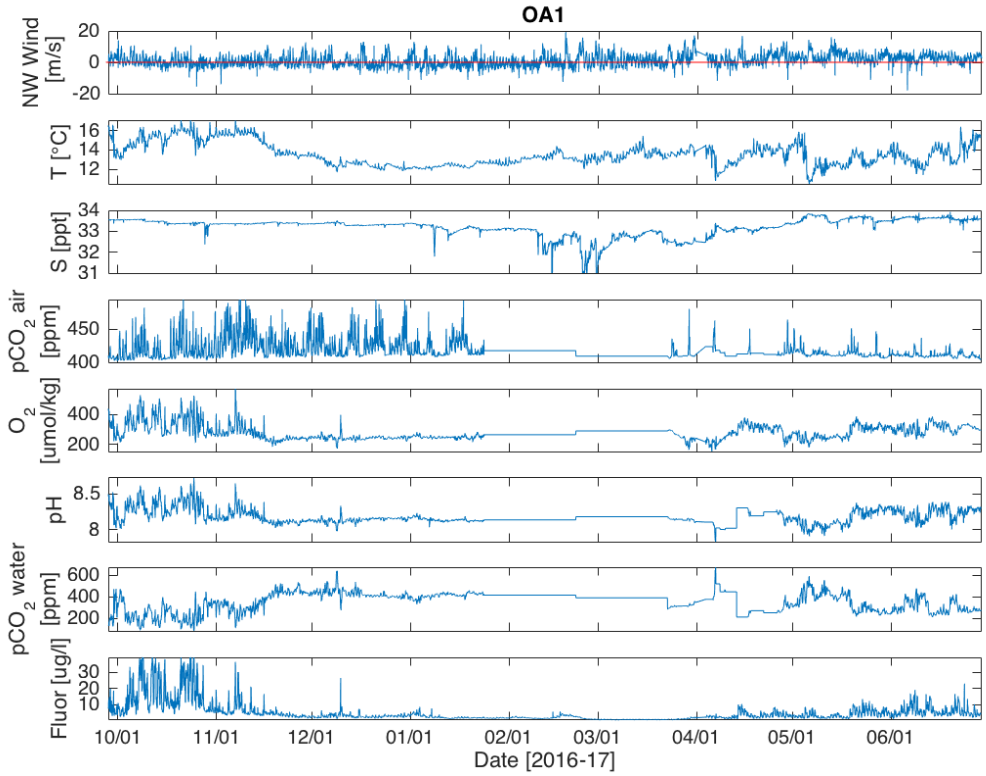
OA1
NW Wind [m/s]
T [°C]
S [ppt]
pCO2 air [ppm]
O2 [umol/kg]
pH
pCO2 water [ppm]
Fluor [ug/l]
Date [2016-17]

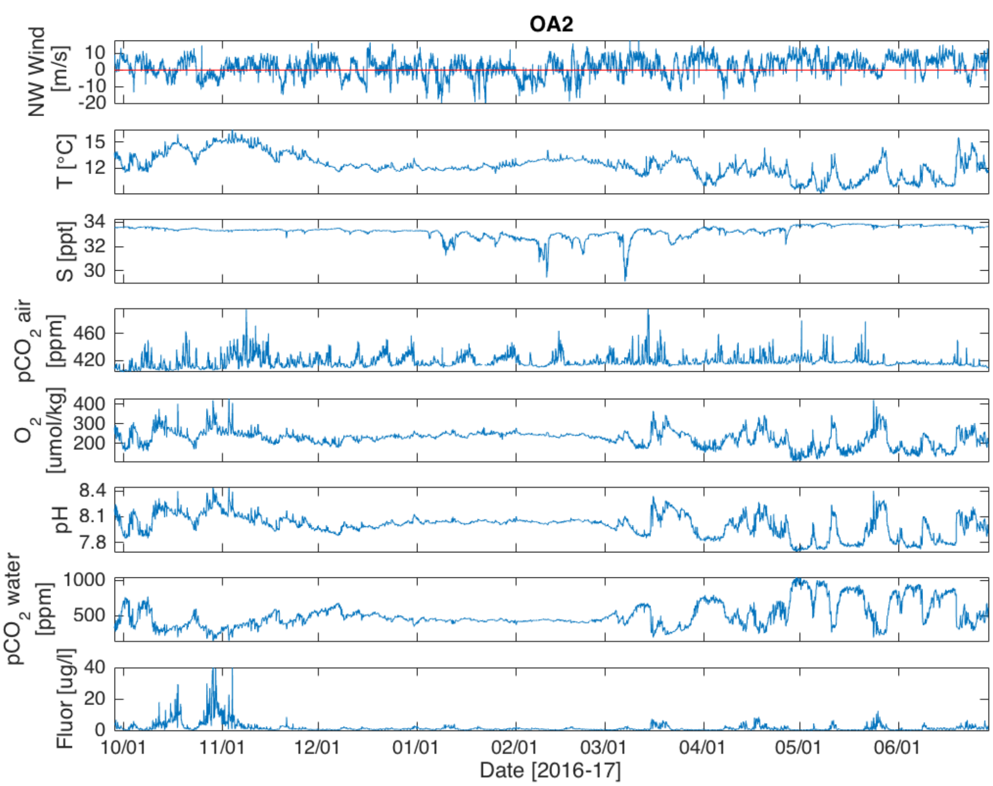
OA2
NW Wind [m/s]
T [°C]
S [ppt]
pCO2 air [ppm]
O2 [umol/kg]
pH
pCO2 water [ppm]
Fluor [ug/l]
Date [2016-17]

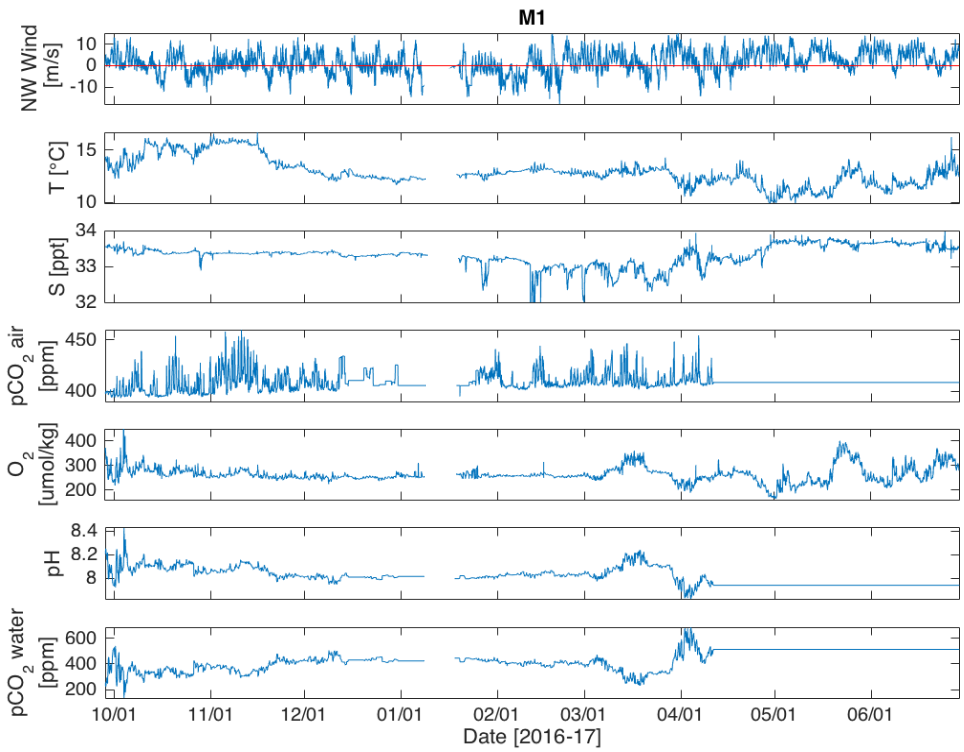

Figure 4. Time series of the three buoys for the September 28, 2016 – June 29, 2017 time period.

The period from December 2016 through March 2017 (Fig. 4) illustrates the low variability of this Davidson Current season described first by Skosberg (1936) and Skosberg & Phelps (1946), and later by Pennington & Chavez (2000). There is low fluctuation in all ocean-driven parameters, which excludes winds, salinity (due to freshwater input) and pCO_2 in air. This suggests that the traces of the Davidson Current described at the end of the first time series (Nov-Dec, 2015), induced by strengthening southerly winds and northward current circulation (Rosenfeld et al., 1994; Pennington & Chavez, 2000), are present in the 3 stations.

This wintertime time series (Fig. 4) shows greater variability in wind direction at all locations, with daily and weekly shifts between negative and positive values of equal strength along the wind's principal axis. This holds true for the Davidson Current period, and transitions to the upwelling season's strong and predominant northwesterly winds around mid March of 2017. During this time period there are also rapid fluctuations between south and north winds, often on a daily scale, with similar strengths that evidence the presence of large winter storms in the region. OA2, as described previously, sees the largest wind speeds, reaching up to 23m/s during southerly wind bursts, while OA1 and M1 observe maxima of 19 and 17 m/s, respectively.

The seasonal trends described for the first time series (Fig. 3) also hold true for temperature in this dataset (Fig. 4). The end of the warm oceanic season (Skosberg, 1936; Skosberg & Phelps, 1946) is observed in the first 6 weeks, followed by cold and stable waters before transitioning into the upwelling season at the end of March and through the beginning of April (Fig. 4). These patterns are evident for the three buoys, which shows that these sites follow the established seasonal patterns of Monterey Bay (Skosberg, 1936; Skosberg & Phelps, 1946; Pennington & Chavez, 2000).

Dissolved oxygen, pH and pCO_2 in seawater have gaps in their data due to sensor failure at different times at OA1 (Hopkins) and M1 (Fig. 4). However, from the data available, and the full OA2 (Año Nuevo) time series (Figs. 2, 3 & 4), the seasonal trends described for the first time period, and seen in temperature variability for this data set, are present. There is little to no relevant variability during the winter months (Fig. 4), and water chemistry begins to change when northwesterly winds strengthen and water temperatures show a cold upwelling signature. However, the second time period has much larger amplitudes for pCO_2 in water at OA2 (Fig. 4, 05/01) than observed in the 2015 time series. The missing data at M1 limits the comparisons between these two sites, but the first measured upwelling event on 04/01 (Fig. 4) suggests that M1 experiences these events at a lag from OA2 and with less strength. OA1 appears to have slightly greater pCO_2 in water variability in 2017 than it did in 2015, but remains much lower than OA2. Comparable pH ranges are seen at the three sites, but the daily and weekly variability remains much larger at OA2. The length of each presumable upwelling event also varies between M1 and OA2, where the signal is clearest, as OA2 tends to remain cold and acidic for longer than M1. These measurements suggest that the strength of the upwelling signal is proportional to the distance from the upwelling center, near OA2.

Salinity shows relatively high variability in all moorings during February and March, changing by up to 2.5 ppt in a single event, as a product of sudden increases in freshwater input to the ocean from record-breaking precipitation in California. At M1, the lowest salinity on 02/11 (Fig. 4) coincides with the last day of a period of 10 rainy days, and a total of more than 4 inches of rain according to Weather Underground's historical data for Watsonville, CA. The same occurs for OA1 and OA2 during this time of high precipitation in the Central California coast. The high variability is only present for the springtime, from February through April, when salinity is also influenced by the transition into the upwelling season and rainfall remains above average. During May and through the end of the time period it shows the same stable, high salinity that is described for the first time period.

The last parameter of interest, pCO_2 in air, shows a trend of high variability during the winter months, a result of stronger southeast winds blowing land pollution to the ocean. The strength of this signal is greater at OA1, as described in the previous time series. OA2 and M1 observe this signal when winds are southerly, at a lag, but also during wind relaxation periods, as evidenced in this time series (Fig. 4: 03/15, 05/20 at OA2; 02/15, 04/01 at M1). Further, detailed analyses of pCO_2 in air are found later in this study. Fluorescence is not analyzed quantitatively because, as a relative measure of biological activity at the surface, it is driven by many parameters, and its correlation with physical parameters is a study unto itself.

2. Analysis of upwelling extremes

The time periods selected for analysis (Figs. 3 & 4) see different upwelling intensities during their peaks in the month of May. This analysis (Table 1) compares the mean, standard deviation, maximum and minimum of temperature, pCO_{2w} and pH for the peak upwelling season of 2015 with the peak upwelling season of 2017. By looking at these extremes, the intensity of two different upwelling seasons is quantitatively compared. The pH and pCO_2 sensors at M1 were not working during May 2017, which limits comparisons for that mooring.

OA1				
May 2015	Mean	Std. Dev	Max.	Min.
Temp. (°C)	13.9	0.6	15.0	12.6
pCO_{2w} (ppm)	276.3	27.4	384.4	222.2
pH	8.16	0.04	8.26	8.01
May 2017				
Temp. (°C)	12.9	1.0	15.9	12.9
pCO_{2w} (ppm)	359.9	88.6	593.0	359.9
pH	8.15	0.12	8.40	8.15

OA2				
May 2015	Mean	Std. Dev	Max.	Min.
Temp. (°C)	11.6	0.6	13.7	10.3
pCO_{2w} (ppm)	501.2	138.3	781.1	245.2
pH	8.00	0.12	8.32	7.79
May 2017				
Temp. (°C)	10.8	1.1	14.7	10.8
pCO_{2w} (ppm)	702.8	232.2	1006.4	702.8
pH	7.88	0.17	8.4	7.88

M1				
May 2015	Mean	Std. Dev	Max.	Min.
Temp. (°C)	12.5	0.5	11.4	14.3
pCO_{2w} (ppm)	388.6	70.6	551.7	270.4
pH	8.07	0.05	8.23	7.93

Table 1. Mean, standard deviation, maximum and minimum of temperature, pCO_{2w} and pH for May 2015 and May 2017 at each mooring.

The comparisons for May 2015 and 2017 at each mooring show the same signal observed in previous analyses (Figs. 3 & 4) suggesting that upwelling during May 2017 was much stronger than during May 2015. The main indicator of this is the high variability, shown by higher standard deviations for the three parameters observed during the later time period. Similarly, pCO_{2w} reaches greater maxima during May 2017 for OA1 and OA2, which suggest that more deep, cold, high pCO_{2w} waters moved to the surface that season. Comparisons between moorings highlight the same pattern observed previously (Figs. 3 & 4), in which OA2 sees the highest effects of upwelling—highest standard deviation for all variables—while M1 and OA1 follow with similar, lower values. These values show the responses of each site to different intensities of upwelling events, and suggest that stronger upwelling seasons lead to more widespread effects in Monterey Bay as the Hopkins mooring sees large increases in variability in 2017. However, these values also suggest that the relative spatial distribution of the effects of upwelling remains the same regardless of the intensity of the event—OA2 always sees proportionally larger effects, followed by M1, and then OA1.

3. Lag and correlation of parameters and wind patterns

In order to quantitatively relate the responses in physical, chemical and biological variables to physical forcing by winds lagged cross-covariance was calculated (Figs. 5-7, Tables 2 & 3). Plots of normalized cross-covariance (correlation between two variables with the sample means subtracted, where the autocovariance at zero lag equals 1) show how wind and other variables measured at each site correlate statistically. Positive correlations suggest that an increase in northwesterly winds correlates with an increase in a particular variable, and vice versa. Negative lags indicate that the change in winds precedes the change in the variable. Maximum covariance coefficients and their corresponding lags were calculated for the peak closest to 0 based on the predominant cycle observed in the correlation plots (Figs. 5-7). These values estimate how correlated each parameter is to the wind, but do not give insight into the duration of their correlation.

3.1. OA1

a)

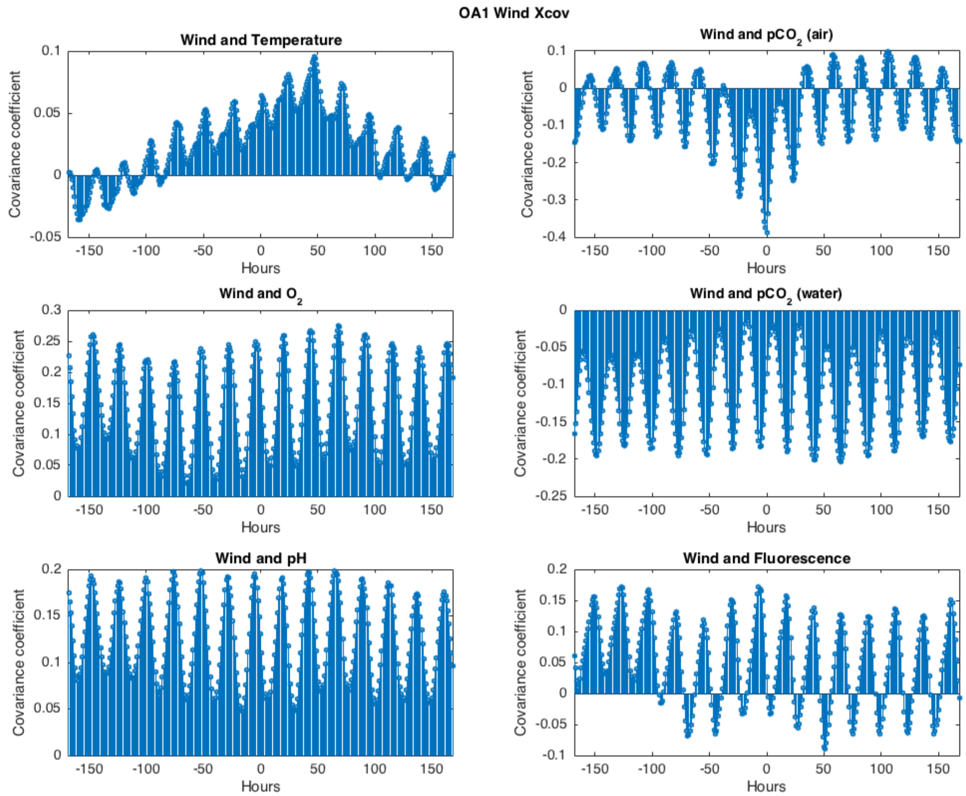

b)

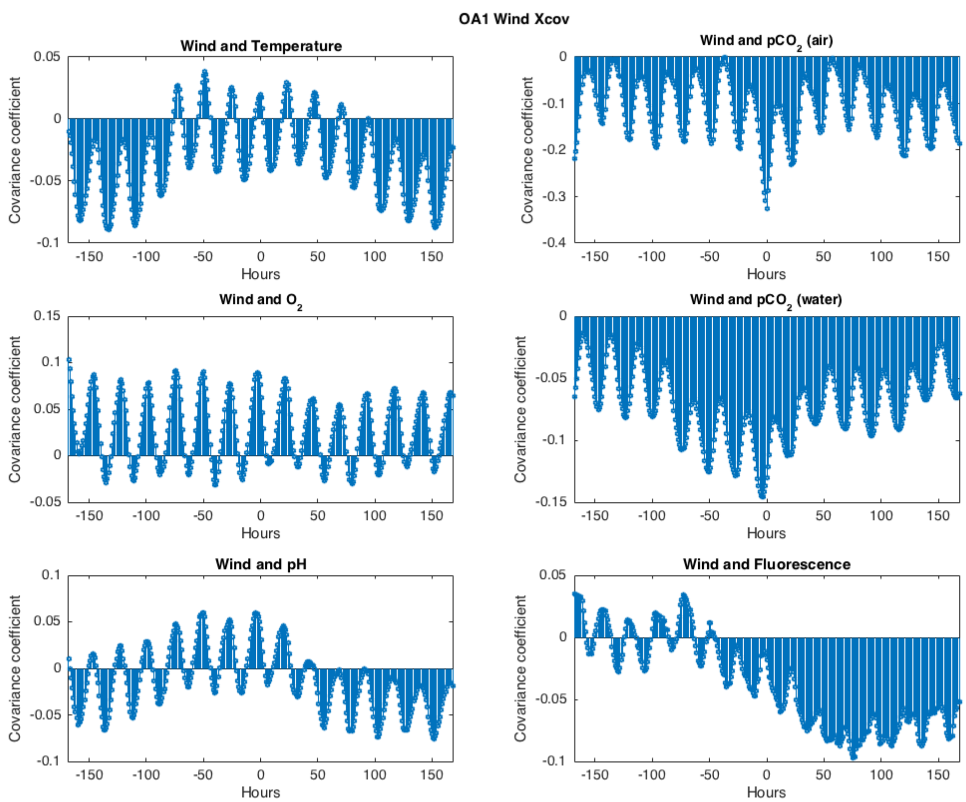

Figure 5. Lagged cross-covariance for two relevant time periods at OA1. a) May 13 – December 7, 2015. b) September 28, 2016 – June, 29 2017.

OA1	May 2015-December 2015		September 2016-June 2017	
	Max. covariance	Lag (hours)	Max. covariance	Lag (hours)
Temp	0.064	1	-0.049	-15
pCO_{2a}	-0.3872	0	-0.326	0
pCO_{2w}	-0.1833	-6	-0.14565	-4
O_2	0.249	-4	0.08875	-3
pH	0.1408	-2	0.0598	-4
Fluor	0.1714	-7	-0.0968	75

Table 2. Maximum cross-covariance and lags between principal wind and various parameters for OA1 at two relevant time periods.

These correlations (Fig. 5 & Table 2) underscore a strong daily (24-hr) cycle that suggests a compounded effect of diurnal winds and biological cycles on these measurements, but further analysis is required to distinguish these two. Positive correlations are present for the 2015 time period between wind and pH and oxygen at lags of 2 and 4 hours respectively at their closest peaks This suggests that, due to the circulation in this part of the bay (Rosenfeld et al., 1994; Paduan & Rosenfeld 1996), as daily northwesterly winds blow toward Monterey at OA1, higher-O_2, higher-pH water moves through OA1, and lower-O_2, lower-pH water piles into the nearshore environment. However, biological activity could also be enhancing this relationship, as diurnal sea breeze increases through the late morning and into the afternoon (Banta et al., 1993) and is followed by peak photosynthesis in the late afternoon (Sournia, 1974). This means that pH and oxygen levels are also affected by biological activity, which has shorter lag times than upwelling-driven processes and could fit the lag times observed at the Hopkins mooring (Table 2).

The correlations for these parameters are much weaker for the October 2016 – July 2017, suggesting that seasonal and annual patterns could also act as sources of variability. The lag time in responses to changes in winds is very short, which, coupled with the low correlation coefficients in most variables compared to OA2 and M1 (Figs. 6 & 7, Tables 3 & 4), further evidence the weak effects of upwelling at OA1.

The correlation between water temperature and wind is the strongest indicator of the predominant diel cycle at OA1, as covariance is positive with a short lag during the May-December time series and negative with a 15 hour lag during the winter time series. This seasonal variation is affected by multiple factors like the pool of warm water in the nearshore environment of the Monterey peninsula near OA1 (Paduan & Rosenfeld, 1996), which dampens cold-water flow. Additionally, water upwelled near the Davenport Upwelling Plume, close to OA2, (Rosenfeld et al., 1994; Pennington & Chavez, 2000) flows to the southeast across Monterey Bay into the peninsula and must displace warmer, stagnant water for OA1 to see significant upwelling signals (Paduan & Rosenfeld, 1996). The temperature correlations at a daily scale (Table 2) have very low values compared to most other parameters, suggesting that the relationship between winds and water temperature at OA1 is not as strong as it is at other locations, and the effects of upwelling are likely to be weak.

However, seawater pCO_2 has a negative correlation with winds that has a stronger signal of high-CO_2 waters characteristic of recently upwelled water. The lags, however, do not align with those observed in the upwelling literature (Service et al., 1998), and suggest that this cycle could also be driven by the diurnal nature of winds and biological activity at OA1. pCO_2 in air does show a strong negative correlation with winds, which means that SE winds blow land CO_2 onto the ocean. This relationship is stronger in the winter, but still very clear during the spring and summer's relaxation periods, and is explored further later in this study.

3.2. OA2

Correlograms at OA2 (Fig. 6) show parameter correlations following a weekly cycle (main peak is within 168 hours and does not repeat), evidence of this buoy's proximity to the upwelling source. Lags for most variables (Table 3) are near the known ranges for upwelling-driven responses (Service et al., 1998), further emphasizing the influence of upwelling on the ocean properties at OA2.

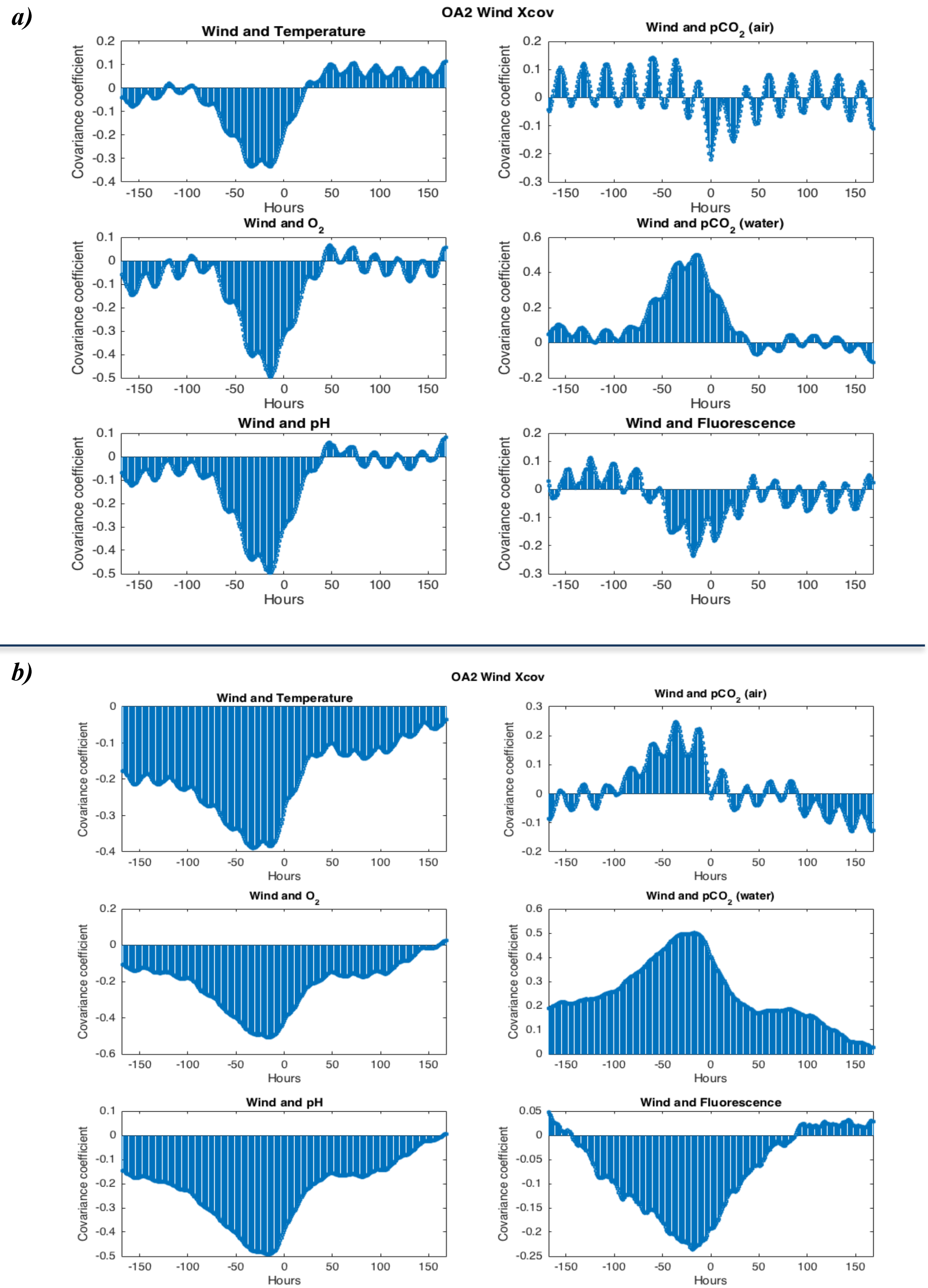

Figure 6. Lagged cross-covariance for two relevant time periods at OA2. a) May 13 – December 7, 2015. b) September 28, 2016 – June, 29 2017.

OA2	May 2015-December 2015		September 2016-June 2017	
	Max. covariance	Lag (hours)	Max. covariance	Lag (hours)
Temp	-0.352	-14	-0.390	-32
pCO_{2a}	-0.221	0	-0.221	0
pCO_{2w}	0.501	-14	0.500	-17
O_2	-0.494	-13	-0.507	-16
pH	-0.496	-14	-0.492	-17
Fluor	-0.238	-18	-0.236	-19

Table 3. Maximum cross-covariance and lags for OA2 between principal wind and various parameters at two relevant time periods.

The correlation coefficients at OA2 are much higher, suggesting a very strong relationship between wind direction and the measured ocean parameters. The only weaker correlation compared to OA1 is pCO_2 in air, a result of the proximity of OA1 to a coastal urban area when southerly winds blow. The strong response to NW winds at OA2 is a result of its proximity to the upwelling source (Rosenfeld et al., 1994, Pennington & Chavez, 2000), which makes its environment highly responsive to upwelled waters. There is also no major difference in covariance between the winter and upwelling season time series, suggesting that these relationships are prevalent year round.

The general trend of a 14-18 hour lag (Table 3) in the correlations for pH, pCO_2 in water and oxygen seems relatively short, as it is lower than the observed lag for the largest wind and temperature correlation. However, the first maxima—of two—for temperature lines up with the peaks of these variables, and all variables correspondingly have a secondary peak at 32-34 hours. This secondary peak is likely a result of the diurnal pattern of coastal winds in this region (Woodson et al., 2007), as the cycle of the sun affects pressure differences by warming air over land, which strengthens winds, and reinforces the upwelling feedback cycle every day the sun heats land. Similarly, the effect of winds on temperature has encompasses a greater period of time than that measured by the lag to the maximum covariance, which suggests that these maximum covariance values do not represent the entire wind-driven effect but only the absolute maximum, which can occur at different lags depending on the upwelling event. If the entire curve for wind and temperature, for example, is observed, the correlation remains strong for a 2-3 day time period, as described in Service et al. (1998). This is also the case for oxygen, pH and pCO_{2w}, suggesting that the maximum covariance of each curve is a descriptive and quantitative, but also arbitrary, measure.

3.3. M1

The correlations at M1 show a weekly event, similar to that of OA2 but with much lower correlation coefficients and different relationships between variables (Fig. 7). This suggests that there is less short-term variability than at OA1, but it isn't as close to the source of upwelling as OA2 to be as strongly correlated to winds (thus not as driven by upwelling events). Due to its location, M1 observes the effects of upwelling as currents flow south, but it is also affected by water circulation over the continental shelf of Monterey Bay, which feeds warmer water from Santa Cruz into the mouth of the bay, (Paduan & Rosenfeld, 1996) and interannual variability driven by freshwater runoff into bay waters (Pennington & Chavez, 2000).

a)

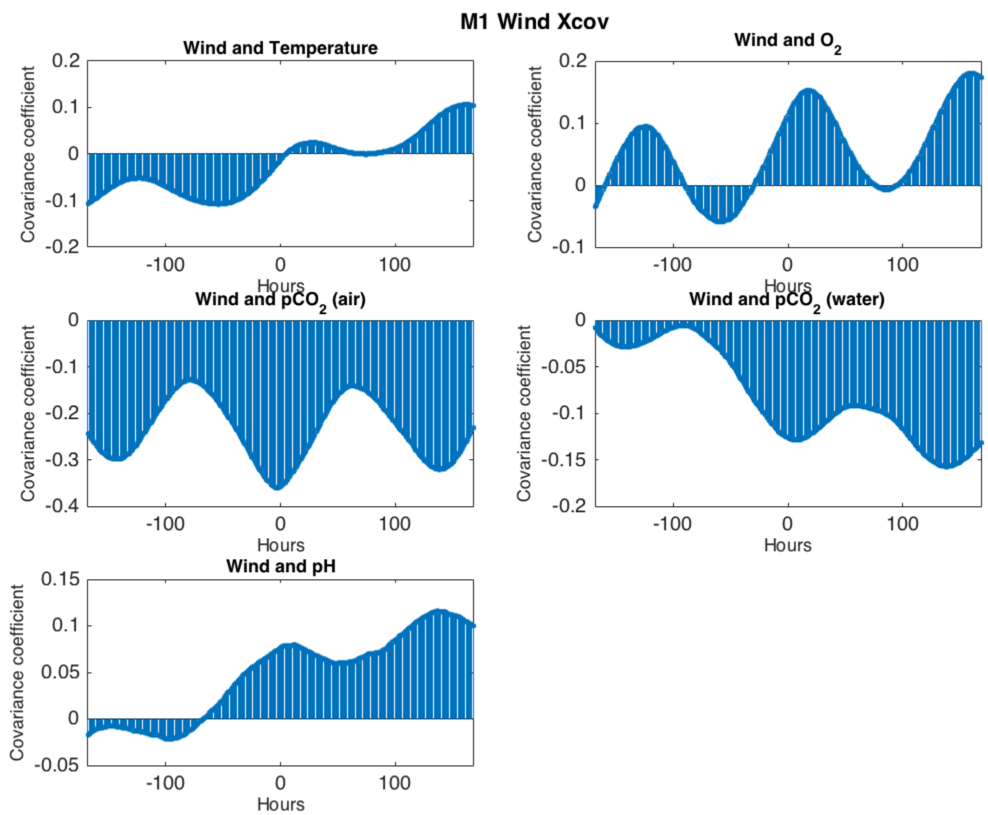

b)

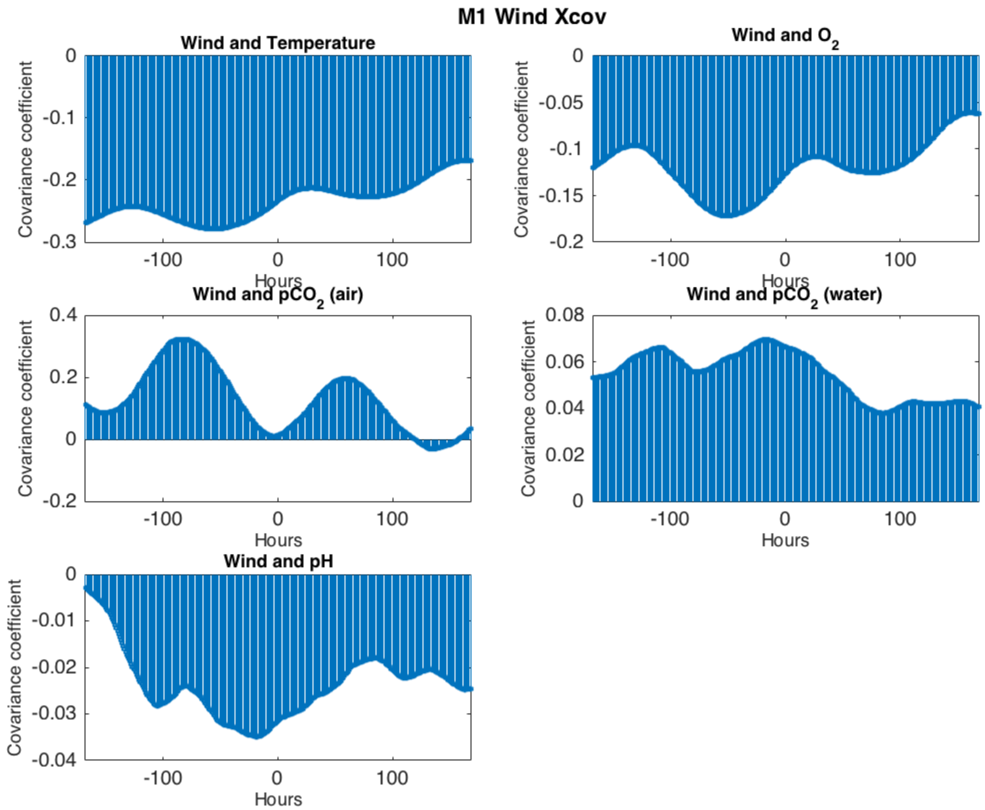

Figure 7. Lagged cross-covariance for two relevant time periods at M1. a) May 13 – December 7, 2015. b) September 28, 2016 – June, 29 2017.

M1	May 2015-December 2015		September 2016-June 2017	
	Max. covariance	Lag (hours)	Max. covariance	Lag (hours)
Temp	-0.1076	-54	-0.2785	-57
pCO_{2a}	-0.3599	-3	0.3223	-84
pCO_{2w}	-0.1482	7	0.0695	17
O_2	0.15276	18	-0.17196	-52
pH	0.0792	12	-0.03488	-19

Table 4. Maximum cross-covariance and lags for M1 between principal wind and various parameters at two relevant time periods.

The correlation with temperature at M1 runs on a 48-hour cycle, which agrees with Service et al.'s (1998) description of these lags. The other variables have a wide range of lag times driven by physical and biological forcing acting in opposite ways. The signal of upwelling is present in water temperature because this property is not affected by biological activity. Oxygen, pH and pCO_{2w} are all affected by biological activity during the ~48 hours it takes water to travel from the upwelling center to M1 (Rosenfeld et al., 1994; Service et al., 1998), which is one of the reasons for lag times to be so wide ranging.

Partial carbon dioxide in air is strongly correlated during both time periods but its lag varies depending on the season. During the May-December, 2015 time series pCO_{2a} decreases after 3 hours of the NW wind activity, but for the October, 2016-July,2017 time series the increase in pCO_{2a} is mostly correlated with NW winds after 84 hours of winds. This could be the same effect caused by southerly winds, which may occur ~84 hours after an upwelling event and increase pCO_{2a} , particularly during the winter time (Figs. 3 & 4)

The correlations are also different than those observed at OA2, particularly with pCO_2 in seawater and pH. During the May-December time period pCO_{2w} has a negative correlation that leads winds (Table 4), which means that pCO_{2w} is lowest around 7 hours before NW winds begin to blow at M1. This correlation shows the expected change in pCO_{2w} , as the lowest value would be expected before winds affect the region. It also suggests that during this time of the year there might not be a conclusive relationship between winds and an increase in pCO_{2w} , as opposed to OA2. This could be due to the constant mixing of old and new water flowing in Monterey Bay, as well as the presence of the Monterey Canyon and biological activity offsetting upwelled pCO_2. The relationship observed during the October 2016 –July 2017 time period for pCO_{2w} has a relatively low correlation value, and suggests that these low correlations, also seen for pH, should be ignored.

4. Extent of responses to diurnal and upwelling-related variability

Two band-pass filters were implemented on all variables at each location to filter extraneous variability and measure diurnal and upwelling driven effects on each parameter. Frequencies chosen for analyses were 23-25 hours (daily) and 3-7 days (upwelling event scale) based on peaks in spectral energy of principle component winds at each location (Fig. 8). The values for the maximum amplitude of the filter are shown as a measurement of the variability at each time scale (Table 5).

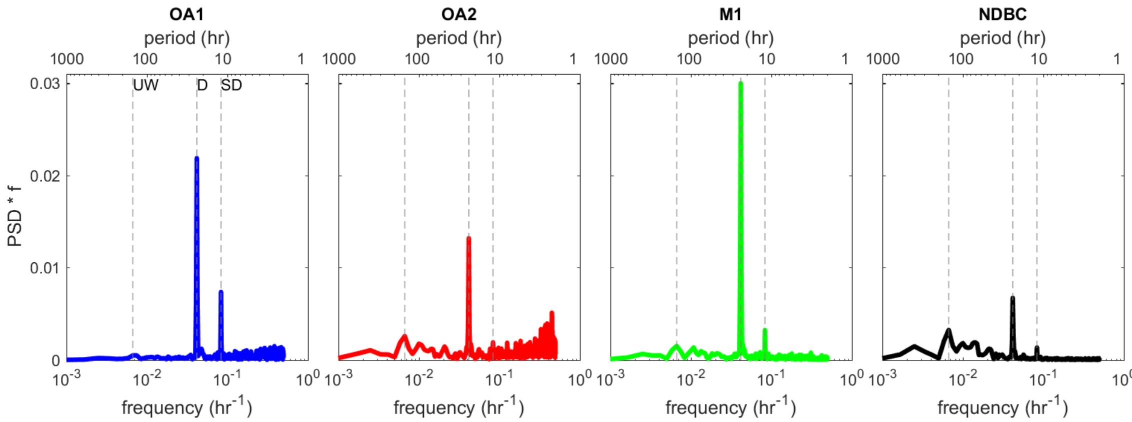

Figure 8. Wind spectra for each location and buoy NDBC 46042, further offshore. UW is 150-hour (~6 day) upwelling frequency, D is 24-hour diurnal frequency, and SD is 12-hour semi-diurnal frequency.

Winds (m/s)			
	OA1	OA2	M1
23-25h	2.6	2.6	4.1
3-7d	5.0	6.0	4.3
Temperature (˚C)			
	OA1	OA2	M1
23-25h	0.2	0.4	0.2
3-7d	0.7	1.6	1.0
Salinity (ppt)			
	OA1	OA2	M1
23-25h	0.03	0.02	0.04
3-7d	0.1	0.1	0.2
O_2 (μmol/kg)			
	OA1	OA2	M1
23-25h	19.3	25.7	13.0
3-7d	18.9	52.8	11.5
pCO_{2a} (ppm)			
	OA1	OA2	M1
23-25h	8.7	10.4	7.8
3-7d	15.3	11.6	8.0
pCO_{2w} (ppm)			
	OA1	OA2	M1
23-25h	40.0	60.1	22.2
3-7d	39.1	167.8	73.7
pH			
	OA1	OA2	M1
23-25h	0.04	0.06	0.02
3-7d	0.05	0.14	0.07

Winds (m/s)			
	OA1	OA2	M1
23-25h	3.8	2.2	3.1
3-7d	5.4	8.9	8.6
Temperature (˚C)			
	OA1	OA2	M1
23-25h	0.3	0.3	0.3
3-7d	1.1	1.7	0.6
Salinity (ppt)			
	OA1	OA2	M1
23-25h	0.2	0.1	0.2
3-7d	0.7	1.1	0.4
O2 (µmol/kg)			
	OA1	OA2	M1
23-25h	39.7	21.7	12.8
3-7d	72.7	55.2	39.7
pCO_{2a} (ppm)			
	OA1	OA2	M1
23-25h	15.5	9.8	12.0
3-7d	13.0	13.9	7.2
pCO_{2w} (ppm)			
	OA1	OA2	M1
23-25h	33.4	31.9	24.3
3-7d	71.0	203.7	62.1
pH			
	OA1	OA2	M1
23-25h	0.06	0.03	0.02
3-7d	0.13	0.15	0.07

Table 5. Maximum band-pass filters amplitudes per variable for each site. (Top) May-December 2015. (Bottom) October 2016 – July 2017.

Wind variability is much higher in the 3-5 day window for OA2 (Table 5), which further shows the effect of upwelling events year round in this location compared to the other sites. M1 has the highest daily wind variability in the upwelling season (Table 5), which coincides with the wind energy spectrum for M1 (Fig. 8), and could be driven by chaotic atmospheric pressure gradients forming nearby due to its exposure to weather. OA1 has the highest daily wind variability for the winter time series, further emphasizing the seasonal period of stabilization at OA2 and M1 during the Davidson Current season.

The amplitudes for temperature show a similar trend for both time periods, in which OA2 fluctuates most in the 3-7 day window, as would be expected due to its proximity to the upwelling center, and least in the daily frequency. OA1 observes slightly larger variability in temperature than M1 during the winter, while M1 fluctuates more during the upwelling period. These amplitudes build on the idea observed previously that suggests that distance from the upwelling center, and local seasonal fluctuations observed in Monterey Bay, are responsible for most of the regional variability present in the area (Figs. 3-7).

The amplitudes of salinity, oxygen, pH and pCO_2 in air and seawater follow the same trends mentioned. OA2 has the largest variability of upwelling-influenced properties like pCO_{2w}, pH and O_2, while OA1 and M1 mostly show similar amplitudes with respect to each other. However, OA1 has the largest daily variability on a yearly basis, as its amplitudes for the 23-25 hour filter are the highest during the winter time series for all variables. This isn't the case for the upwelling season because the extremes observed at M1 and OA2 are much greater due to their respective proximity to the upwelling center.

The amplitudes observed for pCO_{2a} are also noteworthy, as OA1 has higher values during the winter for both filters. This is when southerly winds are most common, and suggests that OA1 is more affected by land pollution than OA2 and M1. OA2 observes similar amplitudes for upwelling and daily scales, and small differences between the spring and winter time series, while M1 and OA1 see higher values during the winter time. This illustrates the influence of the Monterey peninsula's urban centers on OA1 and M1 when the winds blow from the southeast, and it suggests that OA2 doesn't have a significant source of pollution directly in the path of the winds' principal axis of variation. However, further analyses will explore and quantify the extent of the impact of coastal pollution on each mooring.

5. Example of a characteristic upwelling event

The trends described in the previous analyses are best illustrated by observing a 5-day time series of an upwelling event (Fig. 9). The upwelling event of choice is a period of 2 days with strong northwesterly winds in the middle of the summer (June 28 – July 2, 2015), and it illustrates the spatial variability of the effects of upwelling in Monterey Bay.

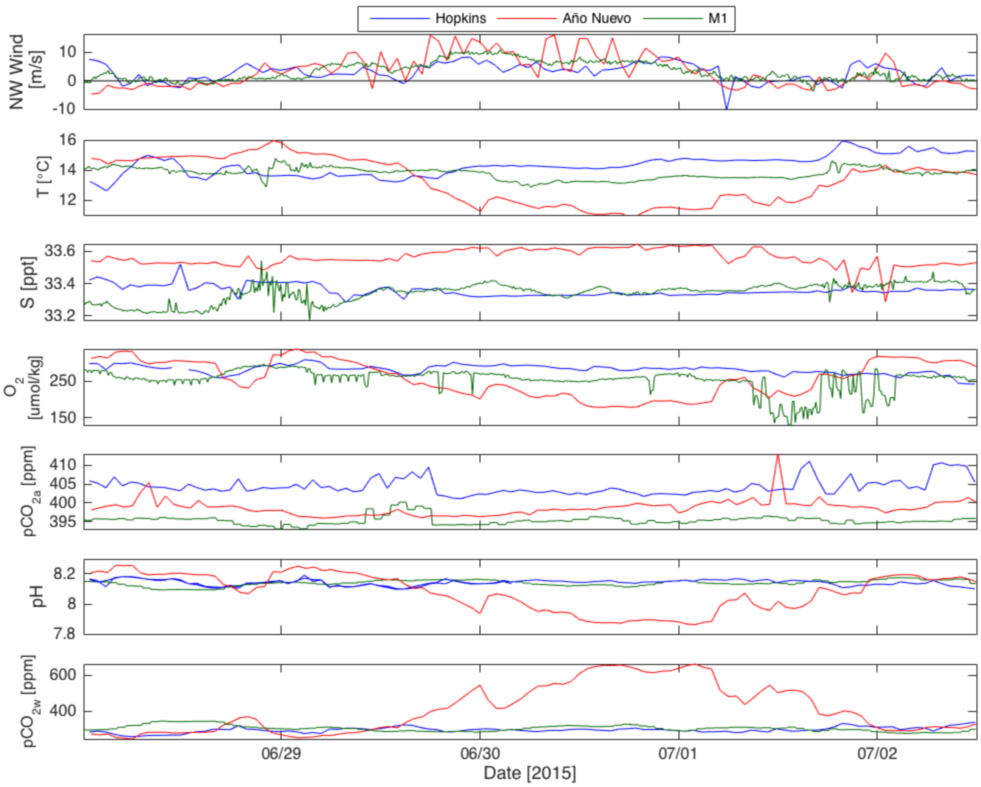

Figure 9. 5-day comparison of a 2-day upwelling event between the three stations.

The 5-day comparison (Fig. 9) illustrates the response of the biological and chemical parameters at each mooring to a two-day upwelling event. It shows the stronger winds present at OA2, and the measurements in response to them. The temperature drops 4 degrees in 24 hours, resulting in a pH drop of 0.2 units and an increase in pCO_2 of about 300 ppm. These responses have been thoroughly described for the Monterey Bay upwelling system (Service et al., 1998; Pennington & Chavez, 2000; García-Reyes et al., 2010), but their regional differences have been mostly observed in terms of current flow (Rosenfeld et al., 1994; Paduan & Rosenfeld, 1996). The hourly timescale of this event illustrates a delayed and weaker response at M1, but suggests that there are measurable impacts of upwelling after a two-day upwelling event. OA1, however, does not observe any changes that could be qualitatively attributed to this single upwelling event.

These plots, in UTC time (Monterey Bay is UTC -7), also illustrate the variability that can be observed within each upwelling event, led primarily by the solar cycle. This partially justifies the high energy in the diurnal frequency of the spectra plots at all stations (Fig. 8).

6. Seasonal variability in daily pH cycle

pH in Monterey Bay has been characterized as driven by low pCO_2 water pulsing from the near shore on internal tides as well as high river run off during rainy seasons (Hofmann et al., 2011). This variability is also coupled with the daily natural photosynthetic cycle driven by biological activity in the region. Time series of 2 and 3 years, with some short intervals without data, were used for each station in this study to look at daily variability averages across each month (Fig. 10). Not all stations had data during the same time periods, which invalidates monthly comparisons between them.

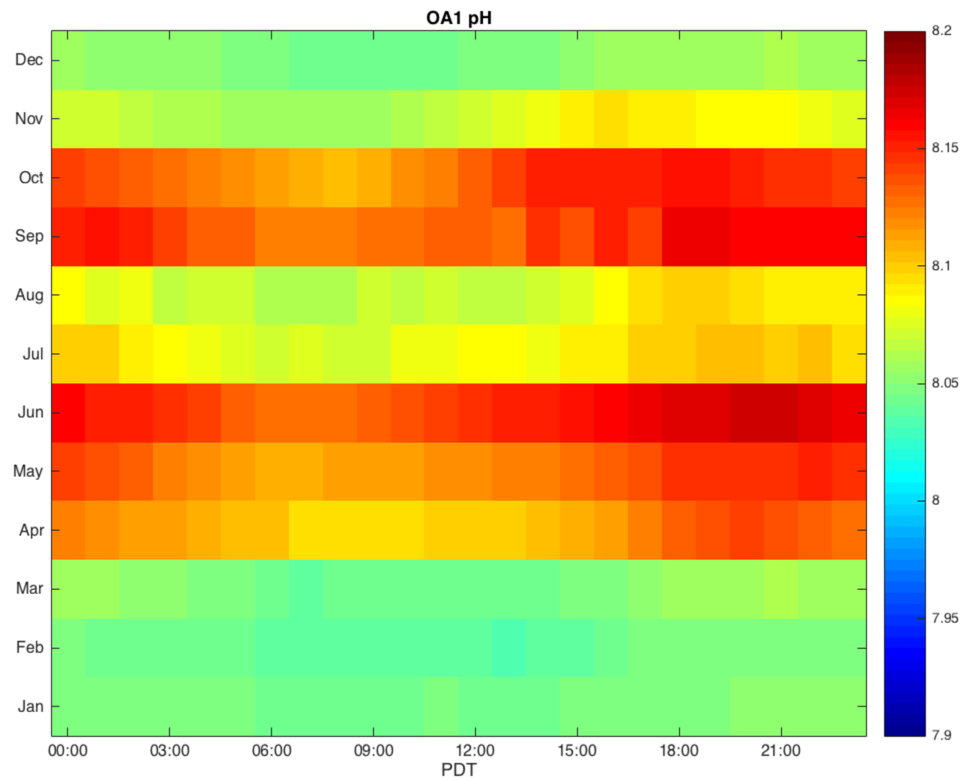

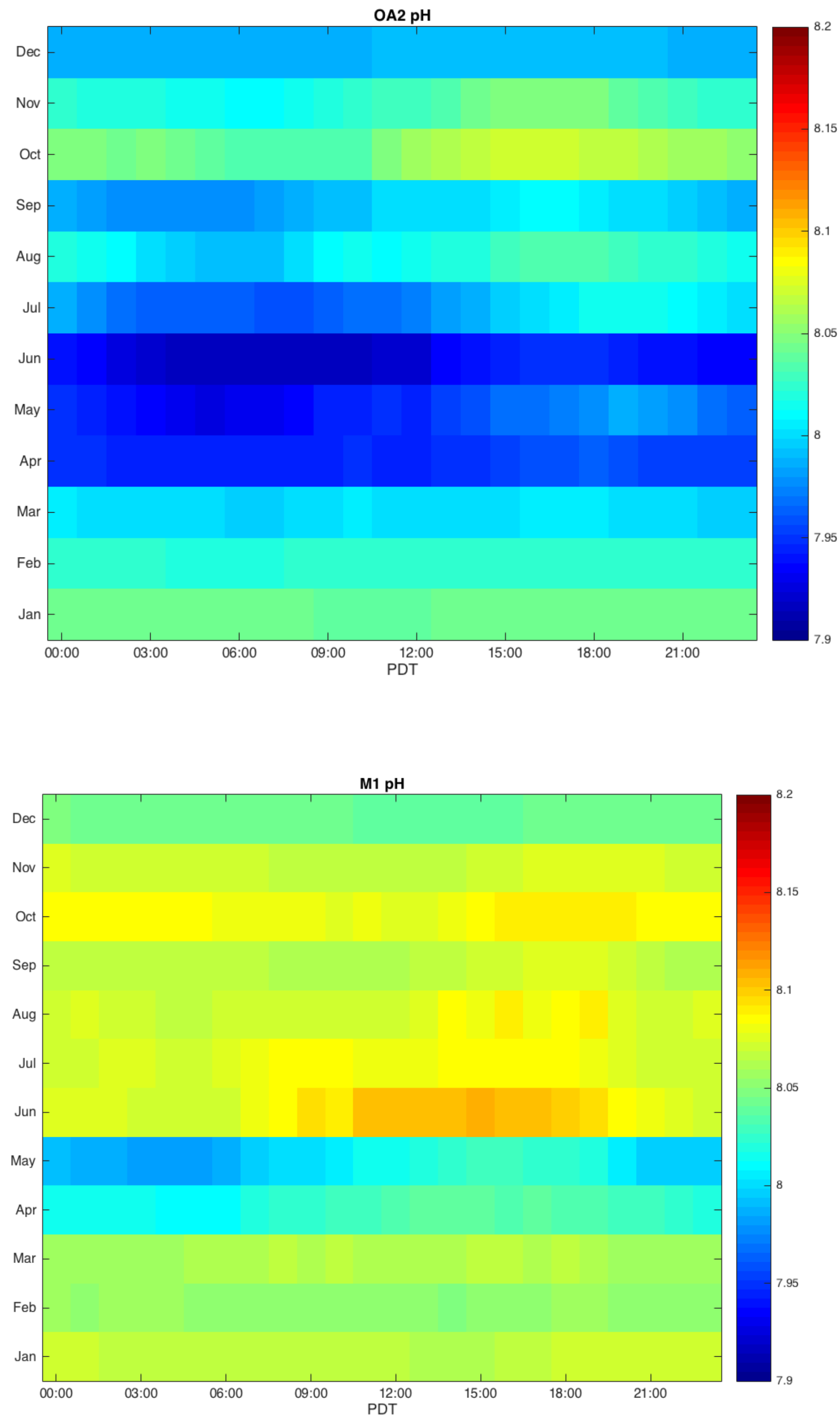

Figure 10. Seasonal variability of daily pH cycle.

There is an evident daily cycle that lengthens and shortens with seasons, as the number of sunlight hours changes. Lower pH relative to the respective month is always found during the earlier times of the day, while higher pH occurs after peak sunlight hours. M1 observes its peak in pH earlier in the day than OA1 and OA2 for the summer months, a result of the competing demands of biological draw-down of CO_2 during daylight hours and the physical forcing of upwelling increasing pH (Service et al., 1998; Pennington & Chavez, 2000; Kudela et al., 2008). This is not observed at OA2 because the effects of biological activity on pH are minimal when compared to those created by the strong upwelling that is evident in the acidic summers at OA2 (Fig. 10). OA1 does not experience any significant acidification during the summer months, an effect of the biological impact on pH in the area and the minimal upwelling that reaches this part of the bay.

Upwelling plays a role in the baseline pH observed during each month, as evidenced at OA2, where the mornings of April-June are the most acidic period of the year. At OA1 and M1, the highest average pH values are often found in the afternoons in summer months during periods of relaxation. This is a result of the physical and biological interactions occurring during this time of the year, as upwelled high-pCO_2 water depends on wind forcing and event duration, which in turn gives way to biological activity, driven by summer's high sunlight levels, during periods of relaxation (Rosenfeld et al., 1994; Service et al., 1998). Following trends observed in previous analyses (Fig. 6, Table 3) OA1 appears to see no significant change in pH caused by upwelling, as its average is driven mostly by the seasonal pattern of biological activity, with the highest pH values throughout the summer—evidencing the lack of an upwelling signal. Similar to the other parameters measured, pH is driven by water circulation in Monterey Bay and distance from the upwelling center (Rosenfeld et al., 1994).

7. The impact of anthropogenic coastal atmospheric pCO_2 in the coastal ocean

Time series and cross-covariance analyses of pCO_{2a} for each mooring (Figs. 3-7; Tables 2-4) suggest a relationship between wind direction and atmospheric carbon dioxide levels. Winds coming from coastal metropolitan areas have been suggested to impact the adjacent coastal zones (Carvalho et al., 2011) but have not been rigorously quantified and are not considered in coastal air-sea flux calculations. The wind roses (Fig. 11) show that winds blowing from nearby urban areas have a greater amount of pCO_2 relative to background atmospheric levels.

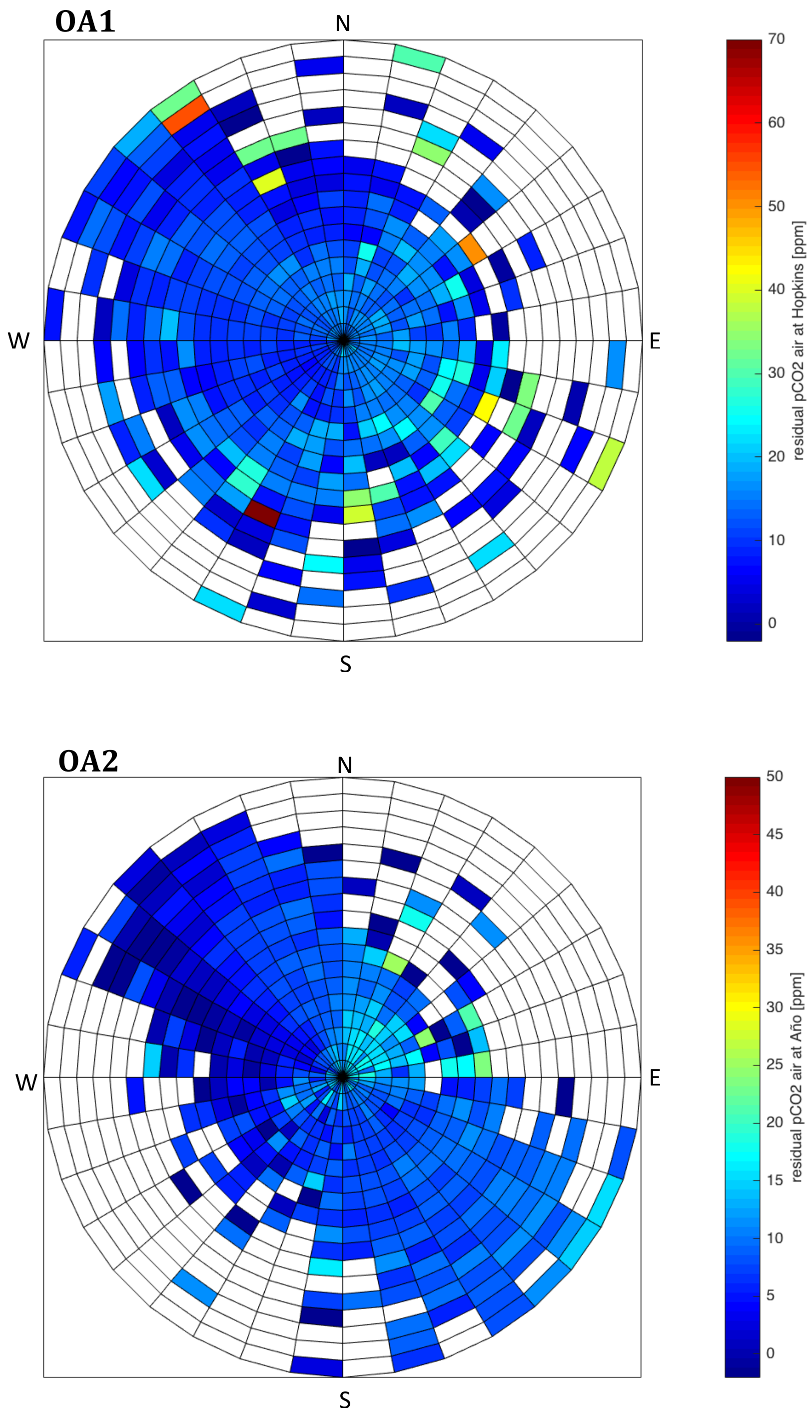

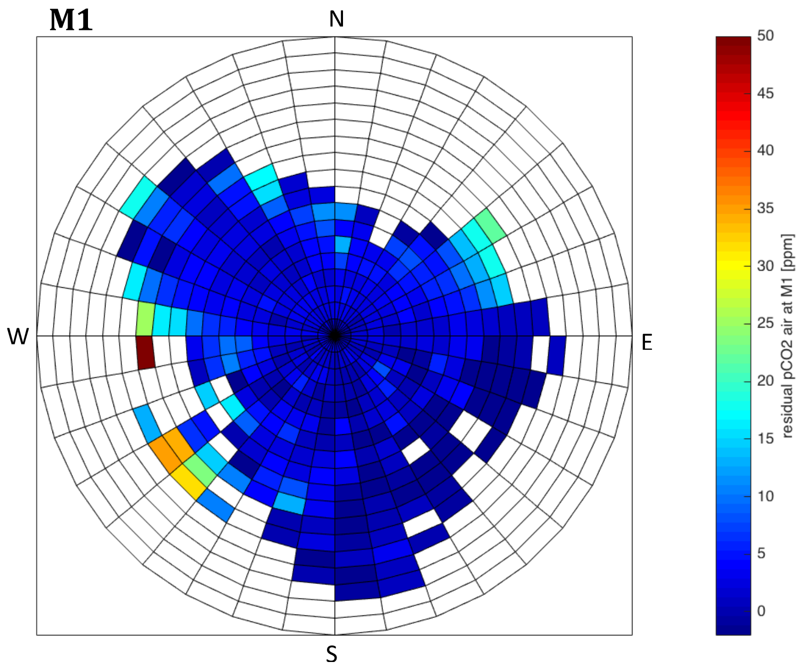

Figure 11. Wind roses showing differences between pCO_{2a} at each mooring and background levels. Wind speed increases radially outward (m/s) and the direction from which the wind blows is in degrees True (0-359).

The differences in pCO_2 suggest that moorings in the coastal ocean can measure the signal of anthropogenic pollution from coastal settlements. At OA1, the strongest signal comes from the E-S window, which is the direction in which the city of Pacific Grove, CA is located relative to the mooring. Despite this figure (Fig. 11, top) having a broader ranging color axis some noise remains present, which could be a result of the Monterey peninsula's topography relative to prevailing wind direction, storm activity, and pollution from neighboring urban areas. At OA2 the signal is more evident as winds from the NE bring higher pCO_2 from the San Francisco Bay Area, and a small southeasterly component suggests that pollution from Santa Cruz, CA could also be observed. At M1, in the middle of Monterey Bay, the strongest signal is from the SW, a common direction of storm activity making its way up the California coast. There is also a moderate signal from the NE, which could be caused by CO_2 coming from the city of Watsonville, CA.

These trends are quantified by examining the wintertime residual pCO_{2a} (measured pCO_{2a} – background levels of atmospheric pCO_2) and the different CO_2 fluxes from the atmosphere into the ocean at each mooring. CO_2 fluxes were quantified using measured pCO_{2a} at each mooring and global anthropogenic trends of pCO_{2a} (mean global atmospheric pCO_2). The difference between both is the total perturbation to CO_2 flux from a locally-polluted atmosphere (Table 6). Upwelling does not occur during this time of the year in Monterey Bay, which allows for the assumption that the higher pCO_{2a} measured by the sensors at each mooring is due to local anthropogenic sources. Positive fluxes represent a net flux into the ocean, and negative fluxes represent a net flux into the atmosphere.

Residuals (ppm)				
	November	**December**	**January**	**February**
OA1	25.7 ±0.4	24.1 ±0.5	25.1 ±0.5	15.7 ±0.4
OA2	16.3 ±0.4	17.6 ±0.3	18.1±0.3	15.1 ±0.3
M1	8.6 ±0.2	6.5 ±0.2	8.8 ±0.2	6.0 ±0.2

CO_2 flux ($\mu mol\ m^{-2}\ d^{-1}$)				
	November	**December**	**January**	**February**
OA1	-1.0 ±0.1	1.4 ±0.2	-1.0 ±0.2	-1.0 ±0.2
OA2	5.3 ±0.5	15.1 ±0.6	4.5 ±0.3	3.2 ±0.2
M1	-1.7 ±0.1	1.5 ±0.1	-2.1 ±0.1	-1.4 ±0.1

CO_2 flux assuming global mean pCO_{2a} in atmosphere ($\mu mol\ m^{-2}\ d^{-1}$)				
	November	**December**	**January**	**February**
OA1	-0.1 ±0.1	2.6 ±0.2	0.5±0.2	0.2 ±0.2
OA2	6.2 ±0.5	16.7 ±0.6	6.7±0.4	5.3 ±0.2
M1	-1.2 ±0.1	2.1 ±0.1	-1.2 ±0.1	-1.1 ±0.1

CO_2 flux perturbation from atmospheric pollution ($\mu mol\ m^{-2}\ d^{-1}$)				
	November	**December**	**January**	**February**
OA1	0.9 ±0.1	1.2 ±0.3	0.5 ±0.3	0.8 ±0.3
OA2	0.9 ±0.7	1.6 ±0.8	2.2 ±0.5	2.1 ±0.3
M1	0.5 ±0.1	0.6 ±0.1	0.9 ±0.1	0.3 ±0.1

Table 6. Residual pCO_{2a}.real mooring CO_2 flux, CO_2 flux assuming global mean pCO_{2a} in atmosphere, and total CO_2 flux perturbation from atmospheric pollution with their respective standard errors during winter months.

Residual pCO_{2a} is highest at OA1, likely due to its proximity to urban areas, and its average is generally about 25 ppm higher than global mean pCO_{2a} during this time of the year. OA2 sees a similar trend but with lower values, around 17 ppm over the background levels. M1 sees lower values of about 7 ppm over background levels, as expected from its location far from the coast.. These data (Table 6) suggest that atmospheric pollution in the form of carbon dioxide follows a spatial gradient, and dissipates over distance, but it still affects the ocean at distances over 15 km away from the coast.

CO_2 flux calculations (Table 6) show how, despite the high exposure to atmospheric carbon dioxide, the measured flux at OA1 is negative for 3 of the 4 winter months. The CO_2 fluxes assuming mean global pCO_{2a} levels in the atmosphere show positive fluxes for 3 of the 4 months and result in a positive net perturbation from atmospheric pollution to CO_2 flux (increased CO_2 absorption by the ocean). This suggests that there is a measurable impact of human coastal atmospheric pollution on air-sea exchange during the winter at Hopkins. At Año Nuevo, likely due to the strong winds it experiences in the winter, fluxes of CO_2 into the ocean are much higher. Ocean intake of atmospheric CO_2 increases if mean global levels of atmospheric pollution are assumed, and total perturbation to CO_2 fluxes is the largest of the three moorings. This could be a result of strong winds and proximity to the coast, when compared to Hopkins and M1. M1 acts as a carbon source during 3 of the 4 months, regardless of if mean global levels of pollution in the atmosphere are assumed. However, the difference between measured atmospheric flux and the modeled flux shows that M1 sees a net positive perturbation in CO_2 flux due to pollution. This illustrates the spatial gradient of coastal anthropogenic CO_2 (Fig. 11, Table 6), which dissipates with distance from shore but still affects M1 during the winter, a site over 15 km from the nearest shore. This analysis shows that anthropogenic coastal atmospheric pollution has a measurable impact on coastal ocean air-sea fluxes that is currently not being accounted for.

SUMMARY and RECOMMENDATIONS

The time series data show a strong seasonal component to upwelling throughout Monterey Bay. The upwelling-induced variability present in Año Nuevo and M1 is stronger during the spring and early summer, as described in the literature. The duration of changes in seawater properties is proportional to the duration of the strong northwesterly winds, although the lag time varies depending on location. The spatial distribution of upwelling in Monterey Bay is also distinct. Cross-covariance analyses show that the lag time for upwelling-induced changes and the strength of their correlations is proportional to the distance from the upwelling center near Año Nuevo. The band-pass filters show upwelling-scale variability being much higher at Año Nuevo than at the sites further away from the upwelling center. The time series example of a two-day upwelling event illustrates these findings, as the strongest response is seen at Año Nuevo, while Hopkins barely sees an effect and the response at M1 is moderate. Seasonal pH measurements suggest that upwelling drives the highly acidic environment near Año Nuevo in the summer. Hopkins does not see this pattern because there is complex biological activity affecting seawater chemistry and upwelled water takes longer to reach southern Monterey Bay, and M1 only sees the cold water signal of upwelling because biological activity balances the effects of physical forcing by the time upwelled water reaches the mooring.

The atmospheric carbon dioxide measurements by the MBARI moorings show that winds originating from near-coastal urban centers significantly increase concentrations of atmospheric CO_2 (up to 120 ppm) relative to the global average atmosphere. The difference is greater for Hopkins, which is located next to an urban area, followed by Año Nuevo, which is influenced by nearby coastal towns, and M1, which sees a smaller difference as it is located in the middle of Monterey Bay. The estimated air-sea carbon fluxes for the winter at each mooring also show that the coastal ocean at Año Nuevo is a sink of atmospheric carbon dioxide during this time of the year. Hopkins and M1 remain as sources of carbon dioxide, despite having pCO_{2a} levels higher than those in the atmosphere. When mean global pCO_{2a} levels are assumed, the total perturbation to CO_2 flux from coastal atmospheric pollution is positive for the three sites (fluxes shift towards more CO_2 going into the ocean), where Año Nuevo sees the highest perturbation, followed by Hopkins and M1. This means that there is a measurable effect of local atmospheric pollution on air-sea fluxes that is not accounted for in current coastal air-sea flux calculations.

These three moorings provide critical observations that, over time, can grow to enhance our understanding of key oceanographic processes. The role of upwelling systems as a seasonal source and sink of atmospheric CO_2 is critical to our understanding of the mechanisms that keep our planet in steady-state equilibrium, and could improve our understanding of future climate change. Future studies should re-calculate global coastal air-sea fluxes considering the effect of coastal pollution and explore the impact of oceanic seasonal, annual and decadal phenomena in our climate system to better understand the future implications of human activity on the planet,

ACKNOWLEDGEMENTS

This study was made possible by MBARI's Summer Internship Program through the funding provided by The David and Lucile Packard Foundation. I also want to acknowledge the years of work of MBARI's Biological Oceanography Group that made this project possible. Individually, I want to thank Linda Kuhnz and Dr. George Matsumoto for their mentoring and planning of the internship program, Jeff Sevadjian for his patience and disposition while teaching me many valuable skills throughout this project, and Dr. Francisco Chavez for his critical insights and help understanding complex oceanographic processes, and the opportunity to experience scientific research at the highest level.

References:

Bakker, D. C. E., De Baar, H. J. W & H. P. J. De Wilde. 1996. Dissolved carbon dioxide in Dutch coastal waters. Marine Chemistry 55.3–4 (1996): 247–263.

Barber, R.T., Smith, R.L., 1981. Coastal upwelling ecosystems. In: Longhurst, A. (Ed.), Analysis of marine ecosystems. Academic Press, New York, pp. 31-68.

Carvalho, R., Barros, N. & P. Duarte. 2011. Impact of Oporto metropolitan area carbon dioxide emissions over the adjacent coastal zone. In: P. Duarte, & J. M. Santana-Casiano, Oceans and the atmospheric carbon content. Springer. doi: 10.1007/978-90-481-9821-42.

Chao, Yi. 2003. A high-resolution surface vector wind product for coastal oceans: blending satellite scatterometer measurements with regional mesoscale atmospheric model simulations. Geophysical Research Letters 30.1: 37–40.

Chavez, F. P., Barber, R. T., Huyer, A., Kosro, P. M., Ramp, S. R., Stanton, T & B. Rojas de Mendiola. 1991. Horizontal advection and the distribution of nutrients in the coastal transition zone off northern California: effects on primary production, phytoplankton biomass and species composition. Journal of Geophysical Research 96 (C8): 14833-14848.

Drake, P. T., McManus, M. A. & C. D. Storlazzi. 2005. Local wind forcing of the Monterey Bay area inner shelf. Continental Shelf Research 25.3: 397–417.

Friederich, G. E., Walz, P. M., Burczynski, M. G. & F. P. Chavez. 2002. Inorganic carbon in the central California upwelling system during the 1997-1999 El Niño-La Niña event. Progress in Oceanography 54 (1–4): 185–203. doi:10.1016/S0079-6611(02)00049-6.

García-Reyes, M. & J. L. Largier. 2010. Observations of increased wind-driven coastal upwelling off central California. Journal of Geophysical Research 115: 1-8.

Graham, W. M., & J. L. Largier. 1997. Upwelling shadows as nearshore retention sites: the example of northern Monterey Bay. Continental Shelf Research 17.5: 509–532.

Hofmann, G. E., Smith, J. E., Johnson, K. S., Send, U., Levin, L. A., Micheli, F., Paytan, A. et al. 2011. High-Frequency Dynamics of Ocean pH: A Multi-Ecosystem Comparison. PLoS ONE 6 (12). doi:10.1371/journal.pone.0028983.

Kudela, R., Banas, N., Barth, J., Frame, E., Jay, D., Largier, J., Lessard, E., Peterson, T. & A. Vander Woude. 2008. New insights into the controls and mechanisms of plankton productivity in coastal upwelling waters of the Northern California Current System. Oceanography 21 (4): 46–59. doi:10.5670/oceanog.2008.04.

Large, W. G., & S. Pond. 1981. Open ocean momentum flux measurements in moderate to strong winds." Journal of Physical Oceanography 1981: 324–336.

Paduan, J.D. & L. K. Rosenfeld. 1996. Remotely sensed surface currents in Monterey Bay from shore-based HF radar (coastal ocean dynamics application radar). Journal of Geophysical Research 101 (1996): 20669.

Pennington, J. T. & F. P. Chavez. 2017. Decade-scale oceanographic fluctuation in Monterey Bay, California, 1989–2011. Deep Sea Research Part II: Topical Studies in Oceanography (In Press): 1–12.

Pennington, J. T. & F. P. Chavez. 2000. Seasonal fluctuations of temperature, salinity, nitrate, chlorophyll and primary production at station H3/M1 over 1989-1996 in Monterey Bay, California. Deep-Sea Research Part II: Topical Studies in Oceanography 47.5–6: 947–973.

Rosenfeld, Leslie K., Schwing, F.B., Garfield, N. & D. E. Tracy. 1994. Bifurcated flow from an upwelling center: a cold water source for Monterey Bay. Continental Shelf Research 14 (9). doi:10.1016/0278-4343(94)90058-2.

Service, S. K., Rice, J. A. & F. P. Chavez. 1998. relationship between physical and biological variables during the upwelling period in Monterey Bay, CA. Deep-Sea Research Part II - Topical Studies in Oceanography 45.8–9: 1669–1685.

Skosberg, T. 1936. Hydrography of Monterey Bay, California. Thermal conditions, 1929-1933. Transactions of the American Philosophical Society 29: 1–152.

Skosberg, T., & A. Phelps. 1946. Hydrography of Monterey Bay, California. Thermal conditions, Part II, 1934-1937. Proceedings of the American Philosophical Society 90: 350–386.

Sournia, A. 1974. Circadian periodicities in natural populations of marine phytoplankton. *Advances in Marine Biology* 12: 325–389.

Strub, P. T., Allen, J. S., Huyer, A. & R. L. Smith. 1987. Large-scale structure of the spring transition in the coastal ocean off western North America. Journal of Geophysical Research 92: 1527–44. doi:10.18276/pzfm.2015.41/2-20.

van Heuven, S., Pierrot, D., Rae, J. W. B., Lewis, E. & D. W. R. Wallace. 2011. MATLAB program developed for CO2 system calculations. Oak Ridge, Tennessee: Carbon Dioxide Information Analysis Center, Oak Ridge National Laboratory, U.S. Department of Energy. doi:doi: 10.3334/CDIAC/otg.CO2SYS_MATLAB_v1.1.

Wanninkhof, R. H. 1992. Relationship between wind speed and gas exchange. Journal of Geophysical Research 97.92: 7373–7382.

Weiss, R. F. 1974. Carbon dioxide in water and seawater: the solubility of a non-ideal gas. Marine Chemistry 2: 203–215.

Woodson, C. B., Eerkes-Medrano, D. I., Flores-Morales, A., Foley, M. M., Henkel, S. K., Hessing-Lewis, M., Jacinto, D. et al. 2007. Local diurnal upwelling driven by sea breezes in northern Monterey Bay. Continental Shelf Research 27 (18): 2289–2302. doi:10.1016/j.csr.2007.05.014.